CMS Physics Analysis Summary

Contact: cms-pag-conveners-susy@cern.ch 2018/06/04

Search for resonant production of second generation sleptons with same-sign dimuon events in proton-proton collisions at $\sqrt{s} = 13$ TeV

The CMS Collaboration

Abstract

A search for resonant production of second generation sleptons ($\tilde{\mu}$, $\tilde{\nu}_{\mu}$) via the R-parity-violating coupling λ'_{211}, in events with two same-sign muons and at least two jets in the final state is presented. While one muon is expected to be produced directly in the slepton decay, the second muon and at least two jets are produced in the subsequent decay of a neutralino or chargino originating from the resonant slepton. The analysis is based on the 2016 dataset of proton-proton collisions at $\sqrt{s} = 13$ TeV recorded with the CMS detector at the CERN LHC, which corresponds to an integrated luminosity of 35.9 fb^{-1}. No significant deviation is observed with respect to standard model expectations. Upper cross section limits are derived in the context of two simplified models representing the dominant signal contributions. The cross section limits are translated into coupling limits for a modified constrained minimal supersymmetric model with λ'_{211} as an additional R-parity-violating coupling. The results impose significantly extended restrictions of the parameter space compared to previous searches for similar models.

1 Introduction

Supersymmetry (SUSY) [1–3] with R-parity violation (RPV) is an attractive extension of the standard model (SM) offering gauge coupling unification, dynamic electroweak symmetry breaking, and a solution to the hierarchy problem. In SUSY scenarios without RPV, supersymmetric particles can only be produced in pairs, and the lightest supersymmetric particle (LSP) is stable. If the LSP is neutral (e.g. the lightest neutralino $\tilde{\chi}_1^0$), experimental signatures at hadron colliders usually involve a large amount of missing transverse momentum due to undetected LSPs. With RPV the situation is different. The LSP can decay back into standard model particles, and the strong exclusion limits for supersymmetric particles from other searches are less relevant. In addition, SUSY models with RPV allow for different production mechanisms, such as the resonant production of sleptons from quarks, which will be investigated in the present analysis.

In a minimal supersymmetric theory, the superpotential can contain lepton- and baryon-number violating terms,

$$W_{LNV+BNV} = \underbrace{\frac{1}{2}\lambda_{ijk} L_i L_j \bar{E}_k}_{LLE\,\text{term}} + \underbrace{\lambda'_{ijk} L_i Q_j \bar{D}_k}_{LQD\,\text{term}} - \underbrace{\kappa^i L_i H_u}_{LH\,\text{term}} + \underbrace{\frac{1}{2}\lambda''_{ijk} \bar{U}_i \bar{D}_j \bar{D}_k}_{UDD\,\text{term}} \quad . \tag{1}$$

The terms associated with the coupling parameters λ, λ', and κ would lead to lepton-number violation, while the one linked to λ'' causes baryon-number violation. A combination of these terms leads to a rapid decay of the proton, which is not observed in nature. To preserve the proton stability, additional symmetries are introduced. A common choice for this symmetry is called R-parity, which forbids all the terms in Eq. 1. However, there are other symmetries that can replace R-parity and keep the proton stable [4, 5]. Supersymmetric theories where no R-parity conservation is imposed are usually called R-parity-violating models. At the LHC, sleptons can be produced from quarks as s-channel resonances via the trilinear LQD term of the superpotential. The coupling strength of this interaction is characterized by λ'_{ijk}, where i specifies the lepton and jk the quark generations. For proton-proton collisions at the LHC, the contributions from the first quark generation are dominant ($j = k = 1$). The lepton index determines which sleptons can be produced via this coupling. It also defines the possible decay modes of the LSP, since all decay modes of the LSP into SM particles have to involve RPV couplings.

The search presented here focuses on production and decays via the RPV coupling λ'_{211}. Starting from a modified version of the constrained minimal supersymmetric model (cMSSM) [6] with λ'_{211} as an additional coupling, the dominant signal contributions leading to a same-sign dimuon pair are shown in Fig. 1. Here, the LSP is assumed to be the lightest neutralino $\tilde{\chi}_0^1$, and all other RPV couplings are set to zero (single coupling dominance). In the diagrams shown in Fig. 1, a smuon ($\tilde{\mu}$) or a muon sneutrino ($\tilde{\nu}_\mu$) is produced from two light quarks and decays into a muon and either a chargino or a neutralino. If the sparticle produced in the slepton decay is not already the LSP, the $\tilde{\chi}_1^\pm$ ($\tilde{\chi}_0^2$) decays into the LSP and a W (Z) boson. All decay chains end with the decay of the LSP into a second muon and two light quarks via an off-shell smuon in an effective three-body decay. Due to the majorana nature of the LSP, the second muon will have the same charge as the first one in 50% of the cases.

Here, a search for resonant production of second generation sleptons ($\tilde{\mu}$, $\tilde{\nu}_\mu$) in final states with a same-sign muon pair and jets is presented. Same-sign dilepton production is rare in the standard model, and is therefore well suited as a signature for new physics searches. The search is based on 35.9 fb^{-1} of $\sqrt{s} = 13$ TeV proton-proton collision data recorded in 2016 with

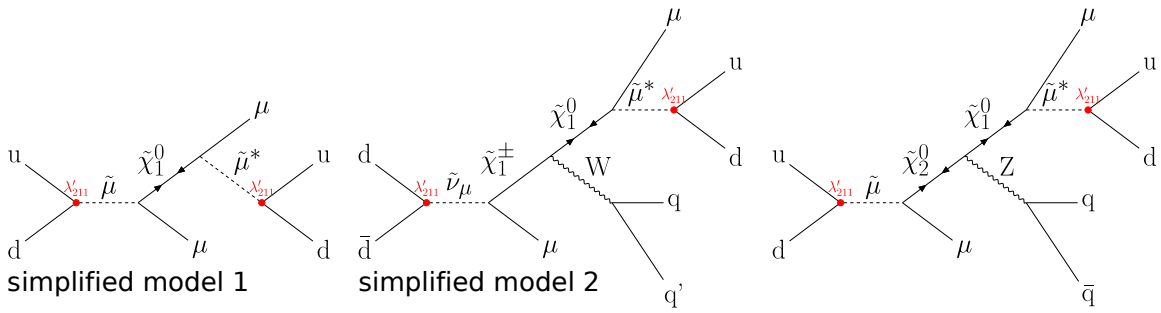

Figure 1: Dominant signal contributions in a modified cMSSM with λ'_{211} as an additional coupling. The left and middle diagrams are simulated as simplified models and considered as signal models for this search.

the CMS detector at the LHC. Limits on resonant production of second generation sleptons have previously been set by the D0 collaboration [7] at the Tevatron.

In the present analysis, a simplified model approach is used, where the dominant signal contributions are extracted and simulated as independent signals. One advantage of this approach is that the final exclusion limits are less model dependent, since the sparticle masses can be set to combinations not allowed in the cMSSM, and the signal contributions are split into the different production mechanisms and decay chains. The left and middle diagrams of Fig. 1 are used as signal models, and will be called simplified model 1 (sm1) and simplified model 2 (sm2) in the following. As long as the W and Z bosons of the diagrams in Fig. 1 decay into light quarks, there is no difference in analysis sensitivity between the middle and right diagrams, and therefore the right diagram will not be considered as an independent signal. To obtain coupling limits for the modified cMSSM, the different contributions from each diagram will be combined based on full model cross sections and branching fractions.

2 The CMS detector and event reconstruction

The central feature of the CMS apparatus is a superconducting solenoid of 6 m internal diameter, providing a magnetic field of 3.8 T. Within the solenoid volume are a silicon pixel and strip tracker, a lead tungstate crystal electromagnetic calorimeter (ECAL), and a brass and scintillator hadron calorimeter (HCAL), each composed of a barrel and two endcap sections. Forward calorimeters extend the pseudorapidity coverage provided by the barrel and endcap detectors. Muons are detected in gas-ionization chambers embedded in the steel flux-return yoke outside the solenoid. A more detailed description of the CMS detector, together with a definition of the coordinate system used and the relevant kinematic variables, can be found in Ref. [8]. Events of interest are selected using a two-tiered trigger system [9]. The first level (L1), composed of custom hardware processors, uses information from the calorimeters and muon detectors to select events at a rate of around 100 kHz within a time interval of less than 4 μs. The second level, known as the high-level trigger (HLT), consists of a farm of processors running a version of the full event reconstruction software optimized for fast processing, and reduces the event rate to around 1 kHz before data storage.

The particle-flow event reconstruction algorithm [10] reconstructs and identifies each individual particle with an optimized combination of information from the various elements of the CMS detector. The energy of electrons is determined from a combination of the electron momentum at the primary interaction vertex as determined by the tracker, the energy of the corresponding ECAL cluster, and the energy sum of all bremsstrahlung photons spatially com-

patible with originating from the electron track. The energy of muons is obtained from the curvature of the corresponding track. The energy of charged hadrons is determined from a combination of their momentum measured in the tracker and the matching ECAL and HCAL energy deposits, corrected for zero-suppression effects and for the response function of the calorimeters to hadronic showers. Finally, the energy of neutral hadrons is obtained from the corresponding corrected ECAL and HCAL energy. Projecting the negative vector sum of all particle flow candidates onto the transverse plane gives the missing transverse momentum vector. The missing transverse momentum ($p_{\mathrm{T}}^{\mathrm{miss}}$) is defined as the magnitude of this vector.

Hadronic jets are clustered from these reconstructed particles using the infrared and collinear safe anti-k_{T} algorithm [11, 12] with a distance parameter of 0.4. The jet momentum is determined as the vectorial sum of all particle momenta in this jet, and is found in the simulation to be within 5 to 10% of the true momentum over the whole p_{T} spectrum and detector acceptance. Jet energy corrections are derived from the simulation, and are confirmed with in situ measurements with the energy balance of dijet and photon + jet events [13]. Before applying jet energy corrections, the contributions from additional proton-proton interactions in the same and previous bunch crossings (pileup) are subtracted. Jets are classified as b-tagged if they pass the medium working point requirements from the combined secondary vertex algorithm (CSVv2) [14].

Muons are measured in the pseudorapidity range $|\eta| < 2.4$, with detection planes made using three technologies: drift tubes, cathode strip chambers, and resistive plate chambers. Matching muons to tracks measured in the silicon tracker results in a relative transverse momentum resolution of 1.3–2.0% for muons with $20 < p_{\mathrm{T}} < 100\,\mathrm{GeV}$ in the barrel, and better than 6% in the endcaps. The p_{T} resolution in the barrel is better than 10% for muons with p_{T} up to 1 TeV [15].

The reconstructed vertex with the largest value of summed physics-object p_{T}^2 is taken to be the primary pp interaction vertex. The physics objects are the jets, clustered using the jet finding algorithm [11, 12] with the tracks assigned to the vertex as inputs, and the associated missing transverse momentum, taken as the negative vector sum of the p_{T} of those jets.

3 Monte Carlo simulation

The MADGRAPH5_aMC@NLO [16] generator is used to simulate the following background processes: $\mathrm{W^{\pm}W^{\pm}}$, $\mathrm{t\bar{t}V}$, $\mathrm{V}\gamma$, $\mathrm{WW}\gamma$, $\mathrm{WZ}\gamma$, $\mathrm{t}\gamma$, $\mathrm{t\bar{t}}\gamma$, VVV, VH, $\mathrm{t\bar{t}t\bar{t}}$ and tZq (V = W, Z). These simulations are done in leading order (LO) [17, 18] or next-to-leading order (NLO) [19] accuracy in terms of perturbative quantumchromodynamics (QCD) and include up to one or two additional partons on matrix element level. For some processes (WZ, ZZ, $\mathrm{t\bar{t}H}$, ggH), POWHEG v2 [20–26] is used instead. Simulations of double parton scattering are done with PYTHIA 8.1 [27]. The parton showering and hadronization is simulated using PYTHIA 8.1 with the CUETP8M1 [28, 29] tune. Double counting of additional partons between MADGRAPH5_aMC@NLO and PYTHIA is removed with the appropriate technique for each simulation (MLM matching for LO [17, 18], FXFX merging for NLO [19]). All samples include a simulation of the contributions from pileup that is matched to the data with a reweighting technique. The parton density functions (PDFs) are NNPDF3.0 LO [30] for LO and NNPDF3.0 NLO [30] for NLO samples, respectively. The GEANT4 [31] package is used to model the detector response for all background processes.

Monte Carlo signal samples are produced for both simplified models defined in Section 1 using MADGRAPH5_aMC@NLO at LO accuracy with NNPDF3.0 LO PDFs and PYTHIA 8.1 for

hadronization and showering. The detector simulation makes use of the CMS fast simulation package [32]. The mass scans range from 200 to 3000 GeV for the slepton mass, and from 100 to 2900 GeV for the LSP mass, with a 100 GeV spacing. For sm2, the mass of the chargino is calculated from the LSP and slepton mass according to Eq. 2 using three different values of x (0.1, 0.5, 0.9):

$$m_{\tilde{\chi}_1^\pm} = m_{\tilde{\chi}_1^0} + x\left(m_{\tilde{\nu}_\mu} - m_{\tilde{\chi}_1^0}\right). \tag{2}$$

For sm2, some points of the scans are omitted since the mass difference between the LSP and $\tilde{\chi}_1^\pm$ would force the W to be virtual. All signal studies are based on the MSSM-RpV-TriRpV model implementation in SARAH [33–36]. Mass spectra, branching fractions, and decay widths have been calculated with SPheno [37, 38].

4 Event selection

Events are selected using triggers that require at least one muon candidate with $p_\mathrm{T} > 50\,\mathrm{GeV}$ within a pseudorapidity of $|\eta| < 2.4$. Typical trigger efficiencies for muons passing the identification criteria described below are around 90%. For events where two muons pass the identification and p_T criteria, this leads to an average efficiency close to 99%.

Events with exactly two well identified muons within the acceptance of $|\eta| < 2.4$ are selected. The p_T of the leading (subleading) muon has to be larger than 60 GeV (20 GeV). In addition, the two muons are required to have the same electrical charge and an invariant mass larger than 15 GeV. The muon reconstruction relies on the results of a global fit using measurements from the silicon tracker as well as the muon chambers. For muon candidates to be well identified, the global fit is required to be geometrically matched to the measurements of the individual subsystems, and the relative uncertainty in the measured muon p_T is required to be smaller than 0.2.

To ensure that muon candidates originate from the primary vertex, the longitudinal and transverse impact parameters must be smaller than 1 mm (0.5 mm). The ratio $|d_\mathrm{3D}|/\sigma(d_\mathrm{3D})$ is required to be smaller than 4. Here, d_3D is the three dimensional impact parameter with respect to the primary vertex.

The isolation criterion for muons is a combination of three different variables ($\mathrm{I_{mini}}$, $p_\mathrm{T}^\mathrm{rel}$, $p_\mathrm{T}^\mathrm{ratio}$) and is designed to provide an efficient selection of muons from heavy particle decays (e.g. W and Z bosons, and SUSY particles) especially in systems with a high Lorentz Boost, where decay products and jets may overlap [39].

The mini isolation ($\mathrm{I_{mini}}$) is defined as the scalar sum of the transverse momenta of neutral hadrons, charged hadrons, and photons inside a cone of $\Delta R = \sqrt{\Delta\eta^2 + \Delta\phi^2}$ around the muon direction at the vertex, divided by the muon p_T. The cone size depends on the lepton p_T as

$$\Delta R\left(p_\mathrm{T}(\ell)\right) = \frac{10\,\mathrm{GeV}}{\min\left[\max\left(p_\mathrm{T}(\ell), 50\,\mathrm{GeV}\right), 200\,\mathrm{GeV}\right]}. \tag{3}$$

The varying isolation cone helps to reduce the inefficiency from accidental overlap between the muon and jets in a busy event environment. The second isolation variable ($p_\mathrm{T}^\mathrm{ratio}$) is defined as the ratio of the muon p_T and the closest jet p_T. If no jet is found within $\Delta R < 0.4$, it is set to 1. The $p_\mathrm{T}^\mathrm{rel}$ variable is defined as the transverse momentum of the muon with respect to the closest jet after subtracting the muon:

$$p_\mathrm{T}^\mathrm{rel} = \frac{|(\vec{p}(\mathrm{jet}) - \vec{p}\,(\ell)) \times \vec{p}(\ell)|}{|\vec{p}(\mathrm{jet}) - \vec{p}(\ell)|}. \tag{4}$$

Muons are classified as isolated if they fulfill the requirements

$$I_{mini} < 0.16 \wedge (p_T^{ratio} > 0.76 \vee p_T^{rel} > 7.2\,GeV). \quad (5)$$

Events are required to contain at least two jets with $p_T > 40\,GeV$ and $|\eta| < 2.4$. Jets that do not pass a set of quality criteria or are within $\Delta R < 0.4$ around a lepton are not included in this number. The quality criteria are designed to reject jets that are likely to originate from anomalous energy deposits. Events with one or more b-tagged jets fulfilling the criteria listed above but with a lowered p_T threshold of 30 GeV are rejected.

Several additional event vetoes are applied. Events with additional muons, one or more electrons, or hadronic taus are rejected. For the muon veto a looser set of identification criteria is used. In addition, the p_T threshold is lowered to 5 GeV and the isolation criterion is replaced by $I_{mini} < 0.4$. Electron identification is based on track quality, the shape of the energy deposits in the ECAL, and the ratio of energy deposits in HCAL and ECAL. Electron candidates with missing hits in the innermost tracking layers or those assigned to a photon conversion are rejected. As an additional criterion, the mini isolation variable for electron candidates (similarly defined as for muons) is required to be smaller than 0.4. All electrons with $p_T > 10\,GeV$ and $|\eta| < 2.5$ and fulfilling the criteria explained above are used for the electron veto. Hadronic tau candidates are reconstructed with the hadron-plus-strips algorithm and identified with a decay mode finding algorithm selecting one- and three-prong decays [40]. The candidates that fulfill the identification criteria, $p_T > 30\,GeV$, and $|\eta| < 2.3$, are used for the tau veto.

To further separate signal and background, the signal region is divided into bins in the $M_{slepton}$-$M_{\tilde{\chi}}$ plane, where $M_{slepton}$ is defined as the invariant mass of the two muons and all selected jets in the event, and $M_{\tilde{\chi}}$ is the invariant mass of the subleading muon and the two leading jets. Events from signal processes would lead to a broad peak around the slepton mass in the $M_{slepton}$ plane. The expected shape of the signal in $M_{\tilde{\chi}}$ is more complicated. Events from sm1 will lead to a peak around the LSP mass in the $M_{\tilde{\chi}}$ distribution. For events from sm2, the behavior depends on the involved masses. While these events will still lead to a broad peak, the peak position will be shifted to higher masses with respect to the LSP mass. This is due to events where one or both of the leadings jets originate from the decay of the W boson instead of the LSP decay. The chosen signal region bins are listed in Table 2.

5 Background estimation

The sources of standard model background contributions can be divided into two classes: processes with two prompt muons and processes with at least one nonprompt muon.

Events from the second class with a same-sign muon pair fulfilling the selection criteria presented earlier are mostly due to the $t\bar{t}$ production process, where one of the muons is produced in the decay of a b hadron and it is thus nonprompt. The contributions of nonprompt muon backgrounds are estimated with the tight-to-loose ratio method. This method has two main steps. First, the ratio of the number of muons passing the tight working point to the number of muons passing the loose one (ϵ_{TL}) is measured in a QCD multijet dominated control region. Here, tight muons are muons fulfilling all selection criteria from Section 4, while loose muons have relaxed constraints on the isolation. This measurement region contains events with exactly one loose muon candidate and at least two jets. To reduce the contamination of prompt leptons in the ϵ_{TL} measurement (mostly from $W \to \mu\nu$), the transverse mass of lepton and p_T^{miss} of events in the control region has to be smaller than 30 GeV. Remaining prompt lepton

contributions are subtracted using MC simulations. In the second step, events from application regions are used as a proxy for the nonprompt contributions to the signal region. Events in these regions have to pass the same requirements as signal region events with the exception that one or both muons fulfill only the loose but not the tight selection criteria. For each muon that is loose but not tight the event is weighted with $\epsilon_{\mathrm{TL}}/(1-\epsilon_{\mathrm{TL}})$. The measurement of ϵ_{TL} is performed as a function of muon η and $p_{\mathrm{T}}^{\mathrm{corr}}$, which is defined as the muon p_{T} corrected according to the amount on energy in the isolation cone above the tight threshold. This is done to reduce the impact of differences between the measurement region (QCD multijet dominated) and the application regions ($\mathrm{t\bar{t}}$ dominated). A detailed explanation of the tight-to-loose ratio method and the definition of $p_{\mathrm{T}}^{\mathrm{corr}}$ is given in Refs. [39, 41].

Processes with two prompt same-sign muons are estimated with MC simulations. The dominant contributions with prompt leptons come from WZ and same-sign $\mathrm{W^{\pm}W^{\pm}}$ production and are labeled as VV in the following. Other important backgrounds arise from $\mathrm{t\bar{t}}$ in association with a W, Z, or Higgs boson ($\mathrm{t\bar{t}V/H}$). The normalization of WZ and $\mathrm{t\bar{t}Z}$ processes is derived from a fit to data using the distribution of the number of b-tagged jets in a control region with three muons, at least two jets, and $p_{\mathrm{T}}^{\mathrm{miss}} > 30\,\mathrm{GeV}$. Two of the tree muons are required to have opposite charge and invariant mass within 15 GeV around the Z mass. This results in scale factors of 1.22 ± 0.14 and 1.15 ± 0.50 for the WZ and $\mathrm{t\bar{t}Z}$ background estimates, respectively.

Another source of standard model background is due to internal photon conversion, where a virtual photon converts into two muons. If the decay is very asymmetric, only one of the muons will pass the muon p_{T} threshold. This kind of conversions combined with the production of e.g. a W boson can contribute to the signal region. The performance of the conversion background simulation is validated in a three lepton control region, where the invariant mass of the opposite sign muon pair closest to the Z mass is smaller than 75 GeV and the invariant mass of the three muons fulfills $|M_{\mu\mu\mu} - M_Z| < 15\,\mathrm{GeV}$. The resulting yields in data and simulation are consistent within the normalization uncertainty assigned to these processes (see Section 6). This background is referred to as $\gamma + X$ in the following.

The remaining sources of background are labeled as 'other' and include VVV, $\mathrm{t\bar{t}t\bar{t}}$, tZq, VH, ggH, and double parton scattering processes.

6 Systematic uncertainties

The expected yields and shapes of background and signal processes are affected by different systematic uncertainties. In Table 1 the uncertainties taken into account for this search are summarized.

Experimental uncertainties include those related to the luminosity measurement, pileup simulation uncertainty, trigger efficiencies, muon identification efficiencies, b-tagging efficiencies and jet energy measurement. These uncertainties are taken into account for both expected signal and background yields. For the luminosity measurement an uncertainty of 2.5% is assigned [42]. The pileup simulation uses the total inelastic cross section, which is varied around its nominal value to obtain an uncertainty estimate. This results in shifts of 0–8% in the expected yields for single signal region bins. The trigger, muon identification and b-tagging efficiencies are measured in data and in the simulation. Differences between the two are corrected by applying scale factors to the simulated events. Uncertainties on these measurements are propagated to the scale factors and used as systematic uncertainties. For the trigger efficiency this results in an uncertainty of 1–2%. The muon identification uncertainty amounts to 3% per muon. For the b-tagging efficiency, the resulting variations are in the range 0–8%. The jet

Table 1: Sources of systematic uncertainties considered in this search and their values and impact ranges in the different signal regions. The background values are given with respect to the processes they concern, while the impacts are normalized to the total event yield in each signal region. For the signal, typical values for the most relevant signal regions are given. The first three blocks affect the backgrounds predictions and list all experimental uncertainties, uncertainties for processes where the yield is obtained from data, and additional uncertainties for simulation based backgrounds. For signal, the first and the last block are relevant.

Source	Value range (%) (background)	Impact range (%) (background)	Typical impact (%) (signal)
Luminosity	2.5	1–2	2.5
Pileup	0–8	0–6	1–3
Trigger efficiency	2	1–2	1
Muon selection	6	3–6	6
b-tagging	1–2	0–2	1–5
Jet energy scale/resolution	1–8	1–8	1–5
Nonprompt muon estimate	32–56	0–21	
Normalization WZ	14	1–3	
Normalization $t\bar{t}Z$	50	0–3	
Scale and PDF variations	5–19	2–18	
Stat. precision of simulations	3–32	3–32	
$W^{\pm}W^{\pm}$ generator comparison	1–25	0–13	
WZ lost lepton	7–24	1–4	
Normalization $\gamma + X$	50	0–13	
Normalization other/$t\bar{t}H$	50	1–7	
ISR uncertainty			0–2
Stat. precision signal efficiency			1–3
Muon efficiencies signal			4

energy measurement in simulation is corrected to match the energy scale and resolution observed in data, where the resulting uncertainties range from 1 to 8%. For the nonprompt muon background estimate several uncertainties are taken into account. The statistical uncertainty due to the finite number of events in the tight-to-loose ratio measurement region and the application region is propagated to the resulting event yields. In addition, uncertainties due to prompt-lepton contamination in the tight-to-loose ratio measurement are considered. In total, this results in uncertainties between 32% and 56% on this background. The fit to obtain the normalization of WZ and $t\bar{t}Z/H$ processes, described in Section 5, results in scale factors with uncertainties of 14% (50%) for the WZ ($t\bar{t}Z$) process, which include statistical and systematic effects.

Theoretical uncertainties are assessed by varying the QCD factorization and normalization scales by factors of 2 and 0.5, respectively. This is done for the main backgrounds estimated from simulation (VV, $t\bar{t}V$). In addition, the different replicas of the NNPDF3.0 [30] set are used to estimate uncertainties due to the proton PDFs. For WZ and $t\bar{t}Z$ only the difference in shape from scale variations is taken into account, since the normalization and its uncertainty are obtained from data. For the less important backgrounds ($\gamma + X$, other, $t\bar{t}H$) a flat 50% normalization uncertainty is used. For the $W^{\pm}W^{\pm}$ background estimate an additional uncertainty is assigned based on the comparison of MADGRAPH and POWHEG predictions for this process. For all processes, uncertainties due to limited sample sizes are taken into account. These are uncorrelated between the signal regions and only affect the shape but not the expected yields.

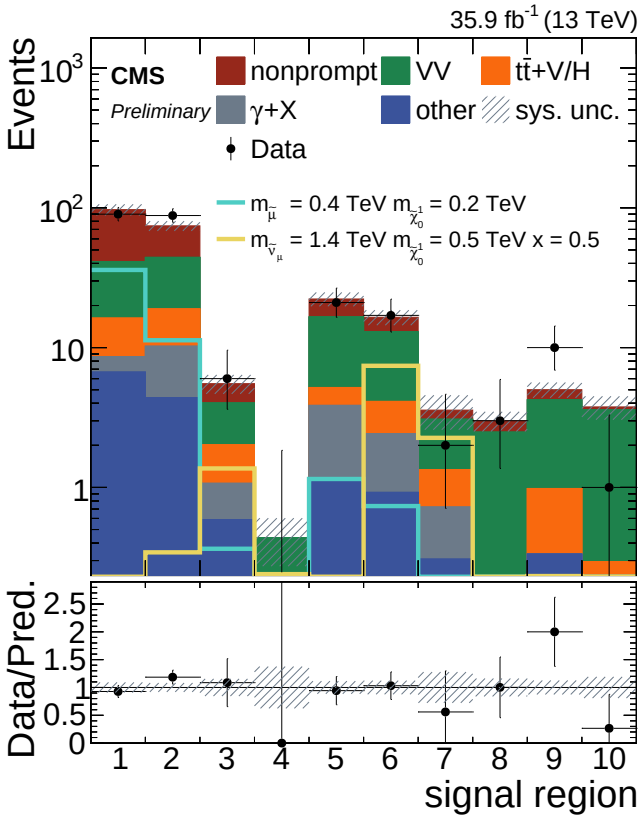

Figure 2: Expected (after fit) and observed event yields in the signal regions as defined in Table 2. The grey band shows the systematic uncertainty on the background yields. Also shown are the expected yields for two signal points normalized to their smallest excluded cross section.

The signal efficiencies and corresponding uncertainties due to limited sample sizes are calculated with the Wilson score interval [43]. The MADGRAPH modeling of initial state radiation (ISR), which affects the total transverse momentum ($p_{\mathrm{T}}^{\mathrm{ISR}}$) of the slepton, is improved by reweighting the $p_{\mathrm{T}}^{\mathrm{ISR}}$ distribution in signal events. The reweighting procedure is based on studies of the transverse momentum of Z events in data [44]. The reweighting factors range between 1.18 at $p_{\mathrm{T}}^{\mathrm{ISR}} = 125\,\mathrm{GeV}$ and 0.78 for $p_{\mathrm{T}}^{\mathrm{ISR}} > 600\,\mathrm{GeV}$. Their deviation from 1.0 is taken as systematic uncertainty on the reweighting. Residual differences between the CMS fast simulation package used for signal samples and the full detector simulation with GEANT4 are corrected by applying additional scale factors. The systematic uncertainties assigned to these scale factors are 2% per muon.

7 Results and interpretation

For the final background estimation, all systematic uncertainties listed in Section 6 are included as nuisance parameters. They are constrained in a maximum likelihood fit of the expected background yields to the observed data in the signal region. For the fit, a signal strength of zero is assumed. The resulting yields after the fit are shown as background estimates for all distributions shown here. The expected and observed yields for the different signal region bins are shown in Fig. 2 and listed in Table 2. The distributions of $\mathrm{M_{slepton}}$ and $\mathrm{M_{\tilde{\chi}}}$ are shown in Fig. 3. No significant deviation is observed with respect to standard model expectations.

Table 2: Expected and observed event yields in the signal regions. The uncertainties are the total systematic uncertainties on the expected yields. Also shown are the expected yields for two signal points normalized to their smallest excludable cross-section.

SR	$M_{\tilde{\chi}}$ (GeV)	M_{slepton} (GeV)	Exp. SM (before fit)	Exp. SM (after fit)	Data	sm1 $m_{\tilde{\mu}}$ = 0.4 TeV $m_{\tilde{\chi}_1^0}$ = 0.2 TeV	sm2 (x=0.5) $m_{\tilde{\nu}}$ = 1.4 TeV $m_{\tilde{\chi}_1^0}$ = 0.5 TeV
1	0–500	0–500	83.0 ± 19.0	97.0 ± 8.9	90	35.9 ± 4.3	< 0.01
2		500–1000	63.0 ± 11.0	74.3 ± 5.9	88	11.3 ± 1.6	0.34 ± 0.05
3		1000–1500	4.84 ± 0.98	5.52 ± 0.85	6	0.37 ± 0.11	1.37 ± 0.18
4		> 1500	0.41 ± 0.15	0.44 ± 0.16	0	0.03 ± 0.02	0.24 ± 0.04
5	500–1000	500–1000	19.7 ± 3.5	22.3 ± 2.5	21	1.16 ± 0.20	0.11 ± 0.02
6		1000–1500	14.5 ± 2.6	16.5 ± 2.0	17	0.74 ± 0.14	7.44 ± 0.86
7		> 1500	4.00 ± 1.30	3.57 ± 0.99	2	0.12 ± 0.04	2.27 ± 0.31
8	1000–1500	1000–1500	2.70 ± 0.57	2.99 ± 0.48	3	0.03 ± 0.02	0.07 ± 0.01
9		> 1500	4.39 ± 0.79	5.00 ± 0.63	10	0.12 ± 0.04	0.23 ± 0.04
10	> 1500	> 1500	3.53 ± 0.84	3.77 ± 0.72	1	0.06 ± 0.03	0.03 ± 0.01

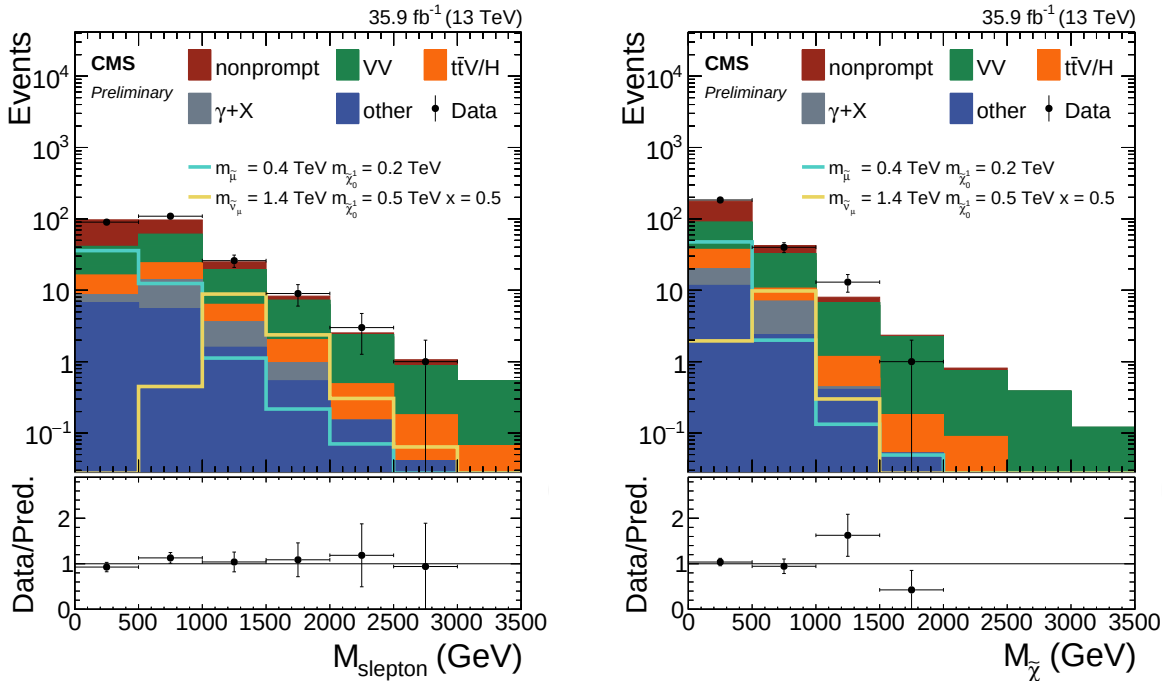

Figure 3: Expected (after fit) and observed event yields in the M_{slepton} and $M_{\tilde{\chi}}$ distribution. Also shown are the expected yields for two signal points normalized to their smallest excluded cross section.

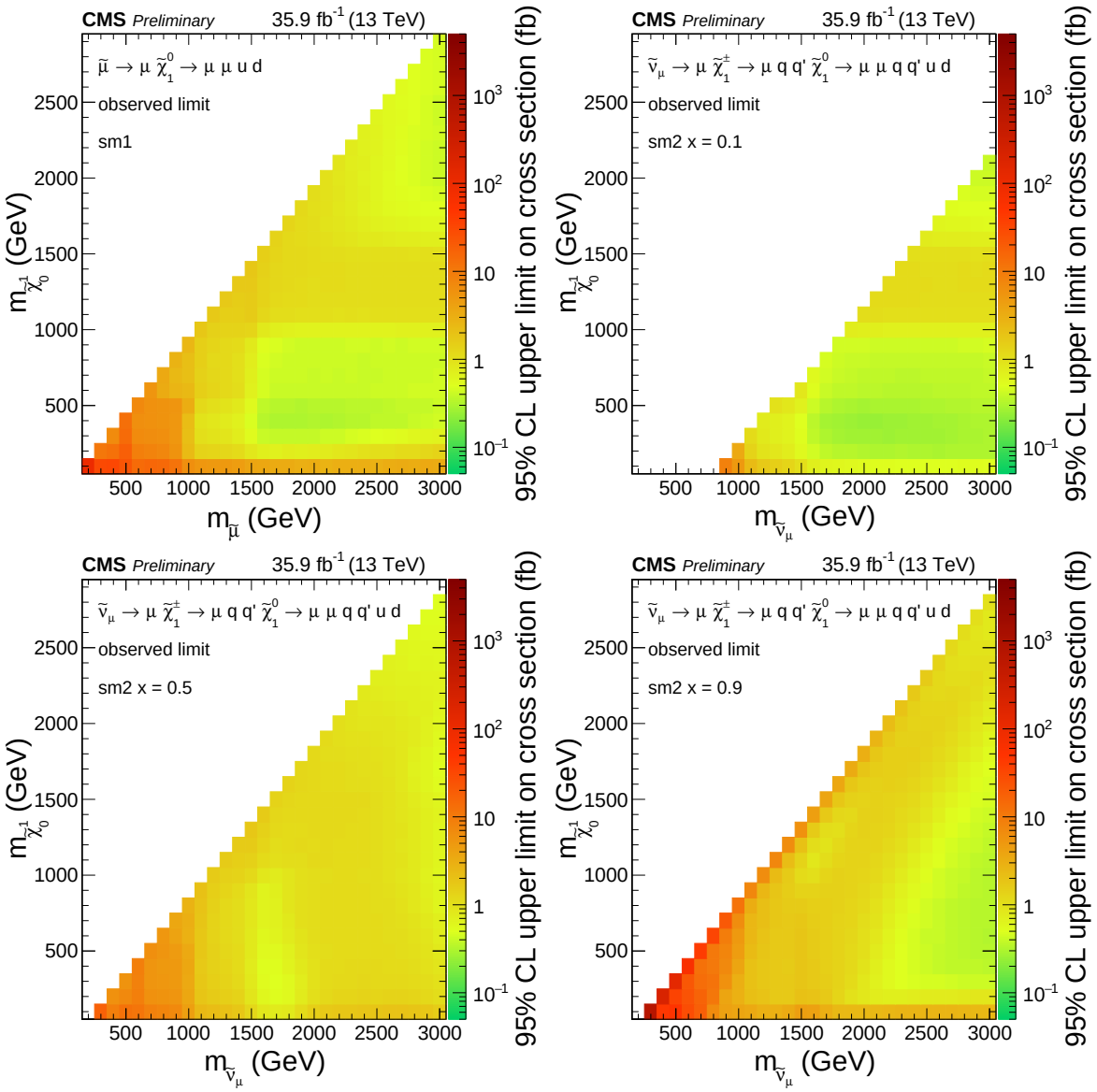

Figure 4: Observed upper cross section limits at 95% CL in the mass plane given by $m_{\tilde{\chi}_1^0}$ and $m_{\tilde{\mu}}$ or $m_{\tilde{\nu}}$ for sm1 or sm2, respectively. The limit for a specific mass combination is depicted according to the color scale on the right-hand side of the figures.

In addition to the background and data yields, two benchmark signal points are shown. The first one is an sm1 signal with $m_{\tilde{\mu}} = 0.4\,\text{TeV}$ and a neutralino mass of $m_{\tilde{\chi}_1^0} = 0.2\,\text{TeV}$. It is normalized to a cross section of 12.8 fb, which corresponds to a coupling of $\lambda'_{211} = 0.0015$ in the modified cMSSM for this process and the chosen masses. The second signal benchmark, from sm2, is normalized to a cross section of 1.1 fb, corresponding to $\lambda'_{211} = 0.0086$. The corresponding slepton mass is 1.4 TeV, the neutralino mass is 0.5 TeV, and $x = 0.5$.

The results are interpreted in terms of the simplified models introduced in Section 1. Upper cross section limits at 95% confidence level (CL) are set using the modified frequentist CLs criterion [45–48]. The uncertainties listed in Section 6 are included as nuisance parameters using lognormal distributions. The observed upper cross section limits are shown in Fig. 4 as a function of the sparticle masses of each signal point.

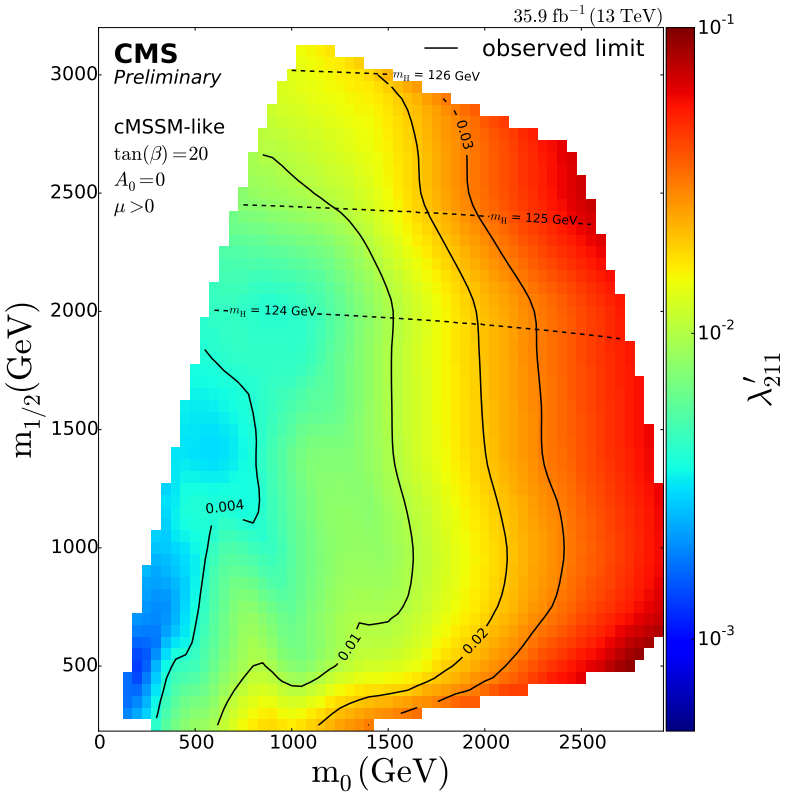

Figure 5: Upper coupling limits as a function of m_0 and $m_{1/2}$ for a modified cMSSM with λ'_{211} as additional RPV coupling. The color scale at the right side of the figure indicates the coupling limit value for specific parameter combinations. These limits are derived from the upper cross section limits of sm1. For four λ'_{211} values (0.004, 0.01, 0.02, 0.03), the coupling limits are shown as black contour line.

The upper cross section bounds are translated into coupling limits of the full cMSSM like model with an additional RPV coupling λ'_{211} as explained in Section 1. This is done for each mass combination of $\tilde{\mu}$ and $\tilde{\chi}_0^1$ in sm1 where the mass combination corresponds to a valid cMSSM point. The λ'_{211} coupling, where the full model cross section times the branching ratio for the decay to sm1 is equal to the observed sm1 cross section limit, is determined. This value corresponds to the smallest excludable coupling. Full model cross sections have been calculated with MADGRAPH for a coupling value of $\lambda'_{211} = 0.01$, with the additional cMSSM parameters $\tan\beta = 20$, $\mu > 0$, and $A_0 = 0$. Cross sections for different coupling values are extrapolated assuming a scaling of the cross section with λ'^2_{211}. Signal points where this assumption is not valid are discarded, e.g. for coupling values where the branching fraction of the $\tilde{\mu}$ or $\tilde{\nu}_\mu$ into quarks becomes relevant. The resulting λ'_{211} limits based on sm1 are shown in Fig. 5. For the cMSSM like model, no constraint on the Higgs mass was imposed. The masses of the lightest Higgs boson in the model are shown as dashed lines. For sm2 points where the three involved masses correspond to a valid cMSSM point, coupling limits are derived in a similar way. These results are listed in Table 3.

8 Summary

A search for resonant production of second generation sleptons ($\tilde{\mu}$, $\tilde{\nu}_\mu$) with 35.9 fb^{-1} of proton-proton collisions recorded in 2016 with the CMS detector has been presented. The search targets resonant slepton production via the RPV coupling λ'_{211} in final states with two same-sign

Table 3: Observed upper coupling limits for the full cMSSM-like model with λ'_{211} as additional coupling based on sm2 points. The masses and upper limits on the cross sections at 95% CL for the corresponding points are also shown.

m_0 (GeV)	$m_{1/2}$ (GeV)	$m_{\tilde{\nu}_\mu}$ (GeV)	$m_{\chi_1^0}$ (GeV)	x	Cross section limit (fb)	λ'_{211} limit
890	250	900	100	0.1	8.8	0.0086
990	250	1000	100	0.1	5.0	0.0081
1880	480	1900	200	0.1	0.33	0.0095
1980	480	2000	200	0.1	0.32	0.011
2670	700	2700	300	0.1	0.28	0.027
2770	700	2800	300	0.1	0.29	0.031
1180	1160	1400	500	0.5	1.13	0.0086
1860	1820	2200	800	0.5	1.14	0.029
2280	2250	2700	1000	0.5	0.93	0.051
2550	2470	3000	1100	0.5	0.63	0.061

muons and at least two jets in the final state. No significant excess over the background expectation is observed. Upper cross section limits are set in the context of two simplified models covering the dominant production mechanisms in a modified constrained minimal supersymmetric model with λ'_{211} as additional coupling. These exclusion limits are translated into λ'_{211} coupling limits. The results represent the most stringent limits on this particular model of RPV SUSY.

References

[1] H. P. Nilles, "Supersymmetry, Supergravity and Particle Physics", *Phys. Rept.* **110** (1984) 1, doi:10.1016/0370-1573(84)90008-5.

[2] H. E. Haber and G. L. Kane, "The Search for Supersymmetry: Probing Physics Beyond the Standard Model", *Phys. Rept.* **117** (1985) 75, doi:10.1016/0370-1573(85)90051-1.

[3] S. P. Martin, "A Supersymmetry primer", *Adv. Ser. Direct. High Energy Phys.* **21** (2010) 1, doi:10.1142/9789814307505_0001, arXiv:hep-ph/9709356.

[4] L. E. Ibáñez and G. Ross, "Discrete gauge symmetries and the origin of baryon and lepton number conservation in supersymmetric versions of the standard model", *Nucl. Phys. B* **368** (1992) 3, doi:10.1016/0550-3213(92)90195-H.

[5] H. K. Dreiner, C. Luhn, and M. Thormeier, "What is the discrete gauge symmetry of the MSSM?", *Phys. Rev. D* **73** (2006) 075007, doi:10.1103/PhysRevD.73.075007, arXiv:hep-ph/0512163.

[6] G. L. Kane, C. Kolda, L. Roszkowski, and J. D. Wells, "Study of constrained minimal supersymmetry", *Phys. Rev. D* **49** (1994) 6173, doi:10.1103/PhysRevD.49.6173.

[7] D0 Collaboration, "Search for resonant second generation slepton production at the Tevatron", *Phys. Rev. Lett.* **97** (2006) 111801, doi:10.1103/PhysRevLett.97.111801, arXiv:hep-ex/0605010.

[8] CMS Collaboration, "The CMS experiment at the CERN LHC", *JINST* **3** (2008) S08004, doi:10.1088/1748-0221/3/08/S08004.

[9] CMS Collaboration, "The CMS trigger system", *JINST* **12** (2017) P01020, doi:10.1088/1748-0221/12/01/P01020, arXiv:1609.02366.

[10] CMS Collaboration, "Particle-flow reconstruction and global event description with the CMS detector", *JINST* **12** (2017) P10003, doi:10.1088/1748-0221/12/10/P10003, arXiv:1706.04965.

[11] M. Cacciari, G. P. Salam, and G. Soyez, "The anti-k_t jet clustering algorithm", *JHEP* **04** (2008) 063, doi:10.1088/1126-6708/2008/04/063, arXiv:0802.1189.

[12] M. Cacciari, G. P. Salam, and G. Soyez, "FastJet user manual", *Eur. Phys. J. C* **72** (2012) 1896, doi:10.1140/epjc/s10052-012-1896-2, arXiv:1111.6097.

[13] CMS Collaboration, "Jet energy scale and resolution in the CMS experiment in pp collisions at 8 TeV", *JINST* **12** (2017) P02014, doi:10.1088/1748-0221/12/02/P02014, arXiv:1607.03663.

[14] CMS Collaboration, "Identification of heavy-flavour jets with the CMS detector in pp collisions at 13 TeV", *JINST* **13** (2018) P05011, doi:10.1088/1748-0221/13/05/P05011, arXiv:1712.07158.

[15] CMS Collaboration, "Performance of CMS muon reconstruction in pp collision events at $\sqrt{s} = 7$ TeV", *JINST* **7** (2012) P10002, doi:10.1088/1748-0221/7/10/P10002, arXiv:1206.4071.

[16] J. Alwall et al., "The automated computation of tree-level and next-to-leading order differential cross sections, and their matching to parton shower simulations", *JHEP* **07** (2014) 079, doi:10.1007/JHEP07(2014)079, arXiv:1405.0301.

[17] J. Alwall et al., "Comparative study of various algorithms for the merging of parton showers and matrix elements in hadronic collisions", *Eur. Phys. J. C* **53** (2008) 473, doi:10.1140/epjc/s10052-007-0490-5, arXiv:0706.2569.

[18] J. Alwall, S. de Visscher, and F. Maltoni, "QCD radiation in the production of heavy colored particles at the LHC", *JHEP* **02** (2009) 017, doi:10.1088/1126-6708/2009/02/017, arXiv:0810.5350.

[19] R. Frederix and S. Frixione, "Merging meets matching in MC@NLO", *JHEP* **12** (2012) 061, doi:10.1007/JHEP12(2012)061, arXiv:1209.6215.

[20] P. Nason, "A New method for combining NLO QCD with shower Monte Carlo algorithms", *JHEP* **11** (2004) 040, doi:10.1088/1126-6708/2004/11/040, arXiv:hep-ph/0409146.

[21] S. Frixione, P. Nason, and C. Oleari, "Matching NLO QCD computations with Parton Shower simulations: the POWHEG method", *JHEP* **11** (2007) 070, doi:10.1088/1126-6708/2007/11/070, arXiv:0709.2092.

[22] S. Alioli, P. Nason, C. Oleari, and E. Re, "A general framework for implementing NLO calculations in shower Monte Carlo programs: the POWHEG BOX", *JHEP* **06** (2010) 043, doi:10.1007/JHEP06(2010)043, arXiv:1002.2581.

[23] T. Melia, P. Nason, R. Rontsch, and G. Zanderighi, "W^+W^-, WZ and ZZ production in the POWHEG BOX", *JHEP* **11** (2011) 078, doi:10.1007/JHEP11(2011)078, arXiv:1107.5051.

[24] P. Nason and G. Zanderighi, "W^+W^-, WZ and ZZ production in the POWHEG-BOX-V2", *Eur. Phys. J. C* **74** (2014) 2702, doi:10.1140/epjc/s10052-013-2702-5, arXiv:1311.1365.

[25] H. B. Hartanto, B. Jager, L. Reina, and D. Wackeroth, "Higgs boson production in association with top quarks in the POWHEG BOX", *Phys. Rev. D* **91** (2015) 094003, doi:10.1103/PhysRevD.91.094003, arXiv:1501.04498.

[26] E. Bagnaschi, G. Degrassi, P. Slavich, and A. Vicini, "Higgs production via gluon fusion in the POWHEG approach in the SM and in the MSSM", *JHEP* **02** (2012) 088, doi:10.1007/JHEP02(2012)088, arXiv:1111.2854.

[27] T. Sjöstrand, S. Mrenna, and P. Z. Skands, "A brief introduction to PYTHIA 8.1", *Comput. Phys. Commun.* **178** (2008) 852, doi:10.1016/j.cpc.2008.01.036, arXiv:0710.3820.

[28] P. Skands, S. Carrazza, and J. Rojo, "Tuning PYTHIA 8.1: the Monash 2013 tune", *Eur. Phys. J. C* **74** (2014) 3024, doi:10.1140/epjc/s10052-014-3024-y, arXiv:1404.5630.

[29] CMS Collaboration, "Event generator tunes obtained from underlying event and multiparton scattering measurements", *Eur. Phys. J. C* **76** (2016) 155, doi:10.1140/epjc/s10052-016-3988-x, arXiv:1512.00815.

[30] NNPDF Collaboration, "Parton distributions for the LHC Run II", *JHEP* **04** (2015) 040, doi:10.1007/JHEP04(2015)040, arXiv:1410.8849.

[31] GEANT4 Collaboration, "GEANT4—a simulation toolkit", *Nucl. Instrum. Meth. A* **506** (2003) 250, doi:10.1016/S0168-9002(03)01368-8.

[32] S. Abdullin et al., "The fast simulation of the CMS detector at LHC", *J. Phys. Conf. Ser.* **331** (2011) 032049, doi:10.1088/1742-6596/331/3/032049.

[33] F. Staub, "SARAH 4 : A tool for (not only SUSY) model builders", *Comput. Phys. Commun.* **185** (2014) 1773, doi:10.1016/j.cpc.2014.02.018, arXiv:1309.7223.

[34] F. Staub, T. Ohl, W. Porod, and C. Speckner, "A Tool Box for Implementing Supersymmetric Models", *Comput. Phys. Commun.* **183** (2012) 2165, doi:10.1016/j.cpc.2012.04.013, arXiv:1109.5147.

[35] M. D. Goodsell, K. Nickel, and F. Staub, "Two-Loop Higgs mass calculations in supersymmetric models beyond the MSSM with SARAH and SPheno", *Eur. Phys. J. C* **75** (2015) 32, doi:10.1140/epjc/s10052-014-3247-y, arXiv:1411.0675.

[36] F. Staub and W. Porod, "Improved predictions for intermediate and heavy Supersymmetry in the MSSM and beyond", *Eur. Phys. J. C* **77** (2017) 338, doi:10.1140/epjc/s10052-017-4893-7, arXiv:1703.03267.

[37] W. Porod, "SPheno, a program for calculating supersymmetric spectra, SUSY particle decays and SUSY particle production at e+ e- colliders", *Comput. Phys. Commun.* **153** (2003) 275, doi:10.1016/S0010-4655(03)00222-4, arXiv:hep-ph/0301101.

[38] W. Porod and F. Staub, "SPheno 3.1: Extensions including flavour, CP-phases and models beyond the MSSM", *Comput. Phys. Commun.* **183** (2012) 2458, doi:10.1016/j.cpc.2012.05.021, arXiv:1104.1573.

[39] CMS Collaboration, "Search for new physics in same-sign dilepton events in proton-proton collisions at $\sqrt{s} = 13\,\text{TeV}$", *Eur. Phys. J. C* **76** (2016) 439, doi:10.1140/epjc/s10052-016-4261-z, arXiv:1605.03171.

[40] CMS Collaboration, "Reconstruction and identification of τ lepton decays to hadrons and ν_τ at CMS", *JINST* **11** (2016) P01019, doi:10.1088/1748-0221/11/01/P01019, arXiv:1510.07488.

[41] CMS Collaboration, "Search for physics beyond the standard model in events with two leptons of same sign, missing transverse momentum, and jets in proton-proton collisions at $\sqrt{s} = 13\,\text{TeV}$", *Eur. Phys. J. C* **77** (2017) 578, doi:10.1140/epjc/s10052-017-5079-z, arXiv:1704.07323.

[42] CMS Collaboration, "CMS Luminosity Measurements for the 2016 Data Taking Period", CMS Physics Analysis Summary CMS-PAS-LUM-17-001, 2017.

[43] R. D. Cousins, K. E. Hymes, and J. Tucker, "Frequentist evaluation of intervals estimated for a binomial parameter and for the ratio of poisson means", *Nucl. Instrum. Meth. A* **612** (2010) 388, doi:10.1016/j.nima.2009.10.156.

[44] CMS Collaboration, "Search for top-squark pair production in the single-lepton final state in pp collisions at $\sqrt{s}$ = 8 TeV", *Eur. Phys. J. C* **73** (2013) 2677, doi:10.1140/epjc/s10052-013-2677-2, arXiv:1308.1586.

[45] T. Junk, "Confidence level computation for combining searches with small statistics", *Nucl. Instrum. Meth. A* **434** (1999) 435, doi:10.1016/S0168-9002(99)00498-2, arXiv:hep-ex/9902006.

[46] A. L. Read, "Presentation of search results: The CL_s technique", *J. Phys. G* **28** (2002) 2693, doi:10.1088/0954-3899/28/10/313.

[47] G. Cowan, K. Cranmer, E. Gross, and O. Vitells, "Asymptotic formulae for likelihood-based tests of new physics", *Eur. Phys. J. C* **71** (2011) 1554, doi:10.1140/epjc/s10052-011-1554-0, arXiv:1007.1727. [Erratum: doi:10.1140/epjc/s10052-013-2501-z].

[48] ATLAS and CMS Collaborations, "Procedure for the LHC Higgs boson search combination in summer 2011", Technical Report ATL-PHYS-PUB-2011-11, CMS-NOTE-2011-005, 2011.